Modelling and Control of the Modular Multilevel Matrix Converter and its application to Wind Energy Conversion Systems

Matias Diaz
U. of Santiago of Chile
Santiago, Chile

Roberto Cárdenas
U. of Chile
Santiago, Chile.

Mauricio Espinoza
U. of Costa Rica
San José, Costa Rica

Andres Mora
UTFSM
Valparaíso, Chile

Pat Wheeler
The U. of Nottingham
Nottingham, UK

Abstract—In the last past years, some countries are enforcing stringent grid codes to regulate the connection of Wind Energy Conversion Systems (WECSs) to the electrical network, mainly because of the high penetration of electric power from this renewable source. Additionally, the trend of wind turbines has shown an ongoing power rating growth, reaching sizes up to 10 MW. Multilevel converters appear then as a promising solution for large WECSs, due to its high reliability, controllability and the capability to reach high power ratings. In this scenario, this paper presents a control strategy for the application of the Modular Multilevel Matrix Converter in Multimegawatts Wind Turbines. Extensive computer simulations and a downscaled laboratory prototype, with twenty-seven power cells, are presented to validate the effectiveness of the proposed control system.

.

Keywords— Wind Turbines, Wind Energy Conversion Systems, Fault Ride-Through Capability, Modular Multilevel Matrix Converter.

I. INTRODUCTION

Wind Energy has become in the industry with greatest and fastest growth among all the renewable energy sources. The wind energy production capacity for the whole world increased exponentially from 17.4 GW in 2000 to 432.4 GW in 2015, positioning wind power as a significant and crucial energy source in areas as China, USA and Europe. Powered 30,5 GW of new installations in China, the global wind power installed in 2015 was 63 GW, representing annual market growth of 22% [1].

It is expected a constant increment of wind power capacity in near future. Truthfully, the European Wind Energy Association (EWEA) plan for the next years is to become wind industry in the most competitive energy source, by 2020 onshore and offshore by 2030. EWEA has stated that "wind power would be capable of contributing up to 20% of EU electricity by 2020, 30% by 2030 and 50% by 2050".

An important part of the required future installed wind power will be offshore based, because of the higher wind-energy potential and the lower environmental impacts. Going offshore implies several technology challenges, mainly regarding reliability, efficiency and upscaling. Considering that hugely expensive platforms must support the total weight of the WECS, the size and weight of components are critical, and possible weight reductions become crucial. What is more, it has been demonstrated that high power wind turbines could reduce the cost structure of offshore WECS, reason why upscaling has become the focus of modern wind energy application and research [2], and why wind turbines manufacturers have been upscaling turbine dimensions.

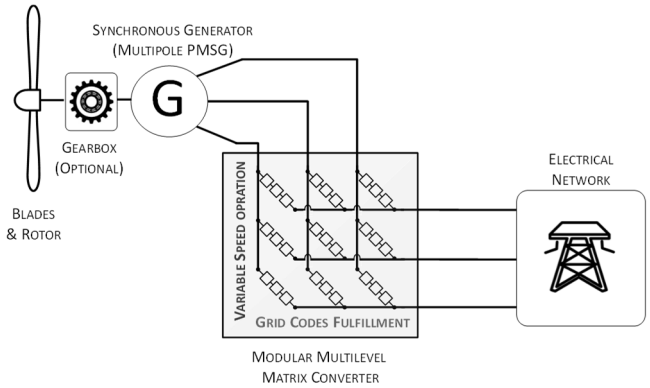

Fig. 1: Proposed topology to drive a High-power Wind Turbines

However, most of the present WECSs are based on low-voltage two-level voltage source power converters (usually based on 1700-V IGBT devices for a 690-V rated output voltage), which is not the best technology for high power applications due to the high currents required. Consequently, medium or high voltage power electronic converters (e.g. multilevel converters) are well suited for high-power wind turbines.Therefore, Modular Multilevel Converters appears as a suitable technology to reach high power ratings.

The M3C is a modular AC/AC converter able to reach medium-voltage levels by the series connection of full-bridge modules. This converter has some advantages compared to traditional two-level converters for high-power applications, fundamentally focused on the full modularity and easy extendibility to reach high voltage and high power levels, redundancy, control flexibility and power quality improvements [3], [4].

In this context, this paper introduces the application of the Modular Multilevel Matrix Converter (M3C) to drive high-power WECSs, as is illustrated in Fig. 1. Comprehensive theoretical discussion on the control and modelling of the M3C is considered. Finally, the effectiveness of the proposed topology is confirmed by experiments using simulation models and a downscaled 5kW laboratory prototype.

GRID INTEGRATION REQUIREMENTS FOR WECS

In countries with a high penetration of renewable energies, dedicated grid code regulations have been enforced to ensure the

Chilean National Fund of Scientific and Technological Development (FONDECYT) grant Nr. 1140337 and the Advanced Centre for Electrical and Electronic Engineering, AC3E, Basal Project FB0008

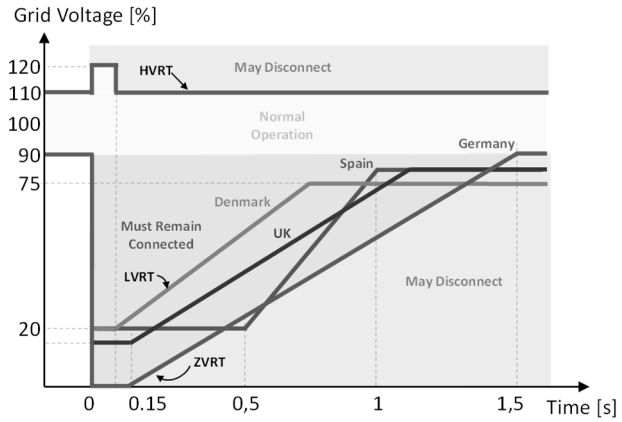

Figure 2: FRT requirements. Voltage profile for simulation of faults in Germany, Denmark, UK and Spain

proper operation of the electrical networks. These grid codes have focused on power quality, power controllability, and Fault Ride Through (FRT) capability. Comprehensive reviews of international grid code requirements for connection of wind turbines to generation and transmission systems are presented in [5]. FRT requirements set the behaviour under Low-Voltage Ride-Through (LVRT) and High-Voltage Ride Through (HVRT) grid-voltages, and represent, likely, the primary concern for wind turbine and power converter manufacturers. As depicted in Fig. 2, FTR from different national grid codes are slightly different in their requirements for the type, magnitude and duration of grid-voltage disturbances:

II. M3C Circuit Configuration

Fig. 3(a) shows the circuit configuration of the M3C, which consists of 9 branches linking the phases of the input system $(a-b-c)$, to the phases of the output system $(r-s-t)$. These branches are the series connection of n Full H-Bridge based cells and one inductor (Fig. 3(b)). The voltage levels and switching frequency of a branch voltage depend on the modulation technique and the number of cells, leading to low low harmonic distortion and small voltage drops when a high number of cells is considered. In this topology, DC capacitor voltages are floating and, therefore, can charge-discharge during the operation of the converter, which means that the average value of all the DC capacitor voltage has to be regulated with low ripple and zero power mean value in steady state operation [16].

To analyse the M3C energy regulation, a single branch as the presented in Fig. 3(b) is used. Neglecting internal losses, the energy stored in a n cells branch is equivalent to the integral of the power at its terminals. Analogously, the energy of a branch is proportional to the capacitor voltages [6]. Therefore, it is possible to determinate the capacitor voltage using the branch power:

$$W_{xy} = \int P_{xy}\, dt \approx \frac{nC}{2}\bar{v}_c^2 \rightarrow P_{xy} \approx nC\bar{v}_c^0 \frac{d}{dt}(\bar{v}_c) \qquad (1)$$

where: $x \in \{a-b-c\}$, $y \in \{r-s-t\}$, P_{xy} represents the branch power. $\bar{v}_c$ is the cluster average capacitor voltage, $\bar{v}_c^0$ is the desired voltage in each cell, the point , n is the number of cells, C represents the capacitance of each capacitor and W_{xy} symbolises the total energy in the n capacitors.

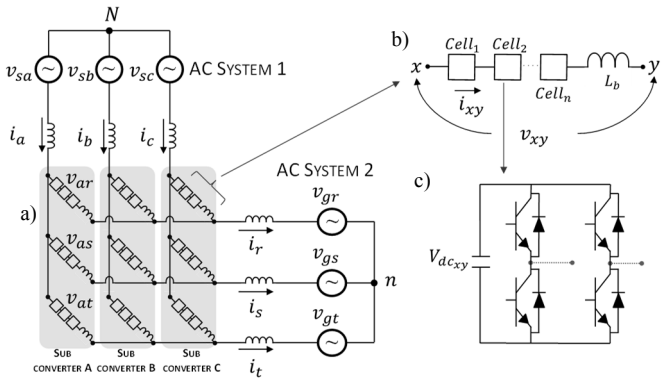

Fig. 3: Modular Multilevel Matrix Converter Topology. (a) Whole converter. (b) M3C Branch composition. (c) M3C Cells.

III. Modelling of the M3C Circuit

Modellings of the M3C have been recently reported in [7], [8], where the fundamental approach is to use a so-called double $\alpha\beta 0$ Transformation. The approach exposed in this paper, is based on [8], but attempts to be an alternative more intuitive.

In a first stage, the input system $(a-b-c)$ is transformed into the $\alpha\beta 0$ reference frame, as is depicted in Fig. 4(a). Afterward, the output systems is transformed into the $\alpha\beta 0$ reference frame. As can be observed in Fig. 4(b), the zero sequence component of v_{ay}, v_{by}, and v_{cy} correspond to the equivalent circuit seen by the output. Analogously, the zero sequence component of v_{xr}, v_{xs}, and v_{xt} can be obtained using the equivalent circuit that the input sees from the converter. It is important to note that the current between points N and n is zero because no path is considered.

Analysing Fig. 4(b), it is possible to write the following equations, which represent a decoupled model for the input, converter and output of the M3C

$$\begin{bmatrix} v_{s\alpha} \\ v_{s\beta} \end{bmatrix} = \begin{bmatrix} v_{\alpha 0} \\ v_{\beta 0} \end{bmatrix} + L_{11}\frac{d}{dt}\begin{bmatrix} i_{s\alpha} \\ i_{s\beta} \end{bmatrix} \qquad (2)$$

$$\begin{bmatrix} v_{g\alpha} \\ v_{g\beta} \end{bmatrix} = \begin{bmatrix} v_{0\alpha} \\ v_{0\beta} \end{bmatrix} + L_{22}\frac{d}{dt}\begin{bmatrix} i_{g\alpha} \\ i_{g\beta} \end{bmatrix} \qquad (3)$$

$$\begin{bmatrix} v_{\alpha\alpha} & v_{\beta\alpha} \\ v_{\alpha\beta} & v_{\beta\beta} \end{bmatrix} = -L_b\frac{d}{dt}\begin{bmatrix} i_{\alpha\alpha} & i_{\beta\alpha} \\ i_{\alpha\beta} & i_{\beta\beta} \end{bmatrix} \qquad (4)$$

where:

$$L_{11} = (L_1 + L_b/3) \qquad (5)$$

$$L_{22} = (L_2 + L_b/3) \qquad (6)$$

The systems described in equations (2)-(4) represents the dynamics of the M3C. Equations (2) and (3) represent the input and output systems, respectively. A precise definition of the circulating currents among the M3C is show in (4). By this means that it is possible to regulate the circulating currents without perturbing the input and output currents.

IV. Proposed Control Strategy for the M3C

The proposed control strategy is based on the model presented in the previous section and provides decoupled control of the input (2), the output (3), and the M3C (4).

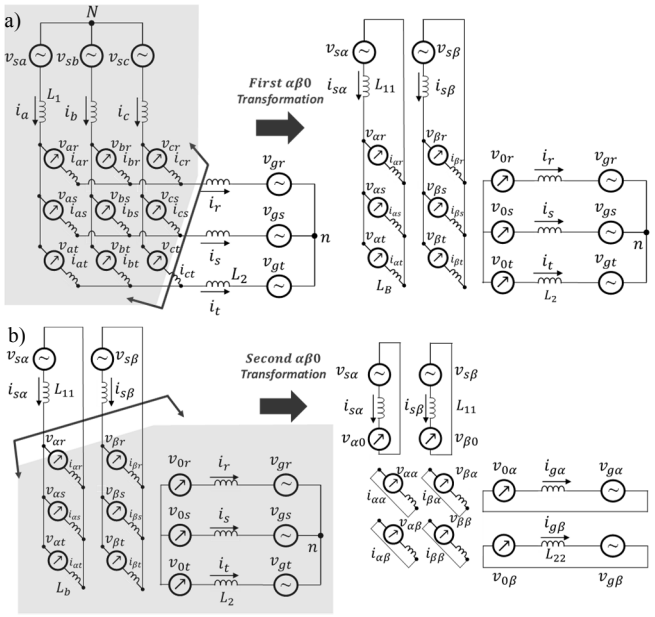

Fig.4: Electric Circuit Modelling of the M3C.

An overview of the proposed control system is presented in Fig. 5, and it is characterised by a hierarchical structure considering the following sub-control systems:

A. Control of the M3C

1) Average Capacitor Voltage Control

From (1), it is possible to express the relationship power/capacitor voltage as:

$$\bar{v}_c = \frac{1}{nC\bar{v}_c^0}\int P_{xy} + \bar{v}_c^0 \tag{7}$$

Using matrix notation (7) yields:

$$\begin{bmatrix} \bar{v}_{c_{ar}} & \bar{v}_{c_{as}} & \bar{v}_{c_{at}} \\ \bar{v}_{c_{br}} & \bar{v}_{c_{bs}} & \bar{v}_{c_{bt}} \\ \bar{v}_{c_{cr}} & \bar{v}_{c_{cs}} & \bar{v}_{c_{ct}} \end{bmatrix} = \frac{1}{nC\bar{v}_c^0}\int \begin{bmatrix} P_{ar} & P_{as} & P_{at} \\ P_{br} & P_{bs} & P_{bt} \\ P_{cr} & P_{cs} & P_{ct} \end{bmatrix} dt + \bar{v}_c^0 \begin{bmatrix} 1 & 1 & 1 \\ 1 & 1 & 1 \\ 1 & 1 & 1 \end{bmatrix} \tag{8}$$

Applying the two-stage $\alpha\beta 0$ transformation:

$$\begin{bmatrix} \bar{v}_{c_{\alpha\alpha}} & \bar{v}_{c_{\beta\alpha}} & \bar{v}_{c_{0\alpha}} \\ \bar{v}_{c_{\alpha\beta}} & \bar{v}_{c_{\beta\beta}} & \bar{v}_{c_{0\beta}} \\ \bar{v}_{c_{\alpha 0}} & \bar{v}_{c_{\beta 0}} & \bar{v}_{c_{00}} \end{bmatrix} = \frac{1}{nC\bar{v}_c^0}\int \begin{bmatrix} P_{\alpha\alpha} & P_{\beta\alpha} & P_{0\alpha} \\ P_{\alpha\beta} & P_{\beta\beta} & P_{0\beta} \\ P_{\alpha 0} & P_{\beta 0} & P_{00} \end{bmatrix} dt + \begin{bmatrix} 0 & 0 & 0 \\ 0 & 0 & 0 \\ 0 & 0 & 3\bar{v}_c^0 \end{bmatrix} \tag{9}$$

When all the elements left side of (8) are equal to $\bar{v}_c^0$, capacitor voltages in the two-stage $\alpha\beta 0$ frame are:

$$\begin{bmatrix} \bar{v}_{c_{\alpha\alpha}} & \bar{v}_{c_{\beta\alpha}} & \bar{v}_{c_{0\alpha}} \\ \bar{v}_{c_{\alpha\beta}} & \bar{v}_{c_{\beta\beta}} & \bar{v}_{c_{0\beta}} \\ \bar{v}_{c_{\alpha 0}} & \bar{v}_{c_{\beta 0}} & \bar{v}_{c_{00}} \end{bmatrix} = \begin{bmatrix} 0 & 0 & 0 \\ 0 & 0 & 0 \\ 0 & 0 & 3\bar{v}_c^0 \end{bmatrix} \tag{10}$$

Therefore, when all capacitor voltages are equal to the desired set-point, just the component "$\bar{v}_{c_{00}}$" has to be regulated. In fact, this component is related to the active power flowing into the converter "P_{00}", that can be expressed as the difference of the input and output converter power and approximated by (9):

$$P_{00} = P_{in} - P_{out} = v_{sd} i_{sd} - P_{out} \approx nC\bar{v}_c^0 \frac{d\bar{v}_{c_{00}}}{dt} \tag{11}$$

Where "v_{sd}" and "i_{sd}" are the d-axis input voltage and current, respectively. Moreover, "P_{out}" could be considered as a perturbation and can be neglected –or feed-forwarded– for control purposes, which lead to the following relationship:

$$i_{sd} = \frac{nC\bar{v}_c^0}{v_{sd}} \frac{d\bar{v}_{c_{00}}}{dt} \tag{12}$$

In consequence, the control system regulates the average voltage of all capacitors by imposing the direct current command i_{sd}^*:

$$i_{sd}^* = G_{PI}(s) * (\bar{v}_{c_{00}}^* - 3\bar{v}_c^0) \tag{13}$$

Where $G_{PI}(s)$ is the transfer function of the PI controller that can be designed using the plant depicted in (12).

2) Balancing Capacitor Voltage Control

The eight remaining components of (10) should be controlled to zero to mitigate the ripple in the capacitor voltages. The unbalance voltage components $\bar{v}_{c_{\alpha\alpha}}$, $\bar{v}_{c_{\beta\alpha}}$, $\bar{v}_{c_{\alpha\beta}}$, $\bar{v}_{c_{\beta\beta}}$ represent the mismatches between capacitor voltages in the same sub converter. On the other hand, components $\bar{v}_{c_{0\alpha}}$, $\bar{v}_{c_{0\beta}}$, $\bar{v}_{c_{\alpha 0}}$, $\bar{v}_{c_{\beta 0}}$ represent the unbalance inter subconverters. In both cases, has been probe that this components can be mitigated either regulating the circulating currents or the common mode voltage v_{Nn}. In this paper, the circulating currents commands have been calculated in order to mitigate the unbalance and oscillating components produced by the variable speed at the input side and to perform inter-subconverter balancing:

$$i_{\alpha\alpha}^* = K_1\left(v_{c_{\alpha\alpha}} sin\theta_m + v_{c_{\beta\alpha}} cos\theta_m\right) + K_2\left(v_{c_{0\alpha}} sin\theta_m\right) + K_3\left(-v_{c_{0\alpha}} sin\theta_g\right) \tag{14}$$

$$i_{\beta\alpha}^* = K_1\left(v_{c_{\alpha\alpha}} cos\theta_m - v_{c_{\beta\alpha}} sin\theta_m\right) + K_2\left(v_{c_{\beta 0}} sin\theta_m\right) + K_3\left(v_{c_{0\alpha}} cos\theta_g\right) \tag{15}$$

$$i_{\alpha\beta}^* = K_1\left(v_{c_{\alpha\beta}} sin\theta_m + v_{c_{\beta\beta}} cos\theta_m\right) + K_2\left(-v_{c_{0\alpha}} cos\theta_m\right) + K_3\left(-v_{c_{0\beta}} sin\theta_g\right) \tag{16}$$

$$i_{\beta\beta}^* = K_1\left(v_{c_{\alpha\beta}} cos\theta_m - v_{c_{\beta\beta}} cos\theta_m\right) + K_2\left(-v_{c_{\beta 0}} cos\theta_m\right) + K_3\left(v_{c_{0\beta}} cos\theta_g\right) \tag{17}$$

Where the constants K_1, K_2 and K_3 are:

$$K_1 = -\frac{\sqrt{6}\, n\, C\, \bar{v}_c}{v_{sd}},\ K_2 = -\frac{\sqrt{3}\, n\, C\, \bar{v}_c}{v_{sd}},\ K_3 = -\frac{\sqrt{3}\, n\, C\, \bar{v}_c}{v_{gd}} \tag{18}$$

moreover, are calculated using the double-stage $\alpha\beta 0$ transformation to the power terms of (8).

3) Circulating Current Control

Because of the topology of the converter, the branch currents, and consequently circulating currents, contain different frequency components (rotating at ω_s and ω_g, which represent the input and output frequencies, respectively). Considering that the plant is integrative, proportional controllers could be well suited for this application. According to (4), the voltage commands to achieve decoupled current control of the four circulating currents should be:

$$\begin{bmatrix} v_{\alpha\alpha}^* & v_{\beta\alpha}^* \\ v_{\alpha\beta}^* & v_{\beta\beta}^* \end{bmatrix} = -K_4\left(\begin{bmatrix} i_{\alpha\alpha}^* & i_{\beta\alpha}^* \\ i_{\alpha\beta}^* & i_{\beta\beta}^* \end{bmatrix} - \begin{bmatrix} i_{\alpha\alpha} & i_{\beta\alpha} \\ i_{\alpha\beta} & i_{\beta\beta} \end{bmatrix}\right) \tag{19}$$

Where K_4 represent the proportional gain transfer function.

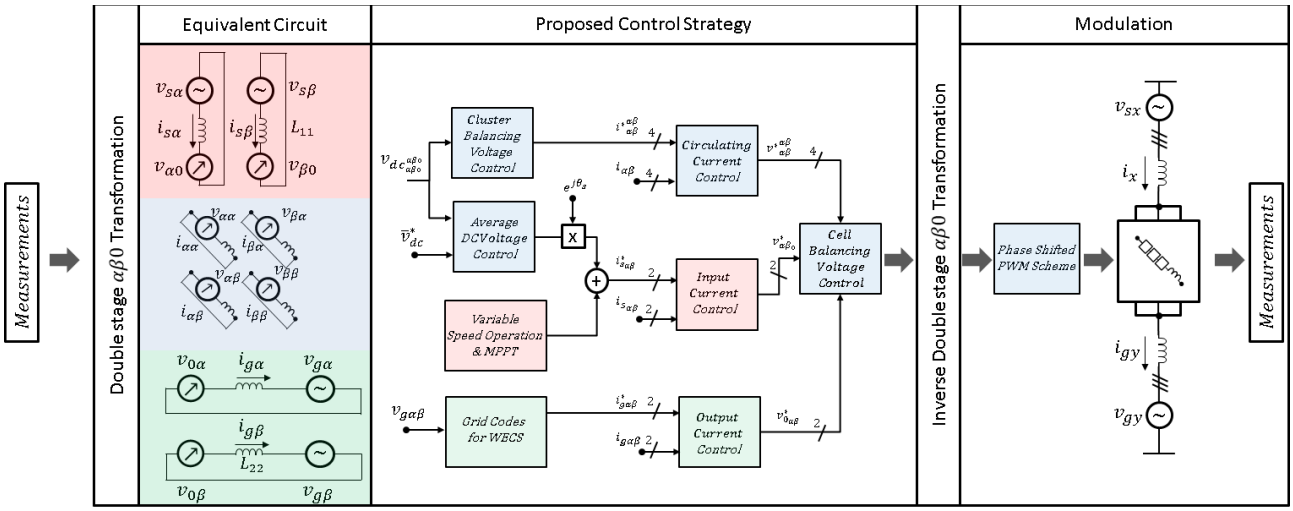

Fig. 5: Overview of the proposed control strategy

B. *Input Current Control:*

In this proposal, the αβ reference frame is used to control the input system. Consequently, the current reference "i_{sd}^*" is transformed into the αβ reference frame the using the input angle θ_s. Besides, using superposition this control scheme can be easily linked with maximum power point tracking control to extract the maximum wind power. The use of a resonant controller is suitable for this application [14]. Considering (2), a simple Resonant Regulator could be utilised to control the input currents as follow:

$$\begin{bmatrix} v_{\alpha 0}^* \\ v_{\beta 0}^* \end{bmatrix} = \begin{bmatrix} v_{s\alpha} \\ v_{s\beta} \end{bmatrix} - L_{11}\frac{d}{dt}\begin{bmatrix} i_{s\alpha} \\ i_{s\beta} \end{bmatrix} + G_{RC_{in}}(s)\left(\begin{bmatrix} i_{s\alpha}^* \\ i_{s\beta}^* \end{bmatrix} - \begin{bmatrix} i_{s\alpha} \\ i_{s\beta} \end{bmatrix}\right) \quad (20)$$

Where $G_{RC_{in}}(s)$ represents the input current Resonant Controller transfer function.

C. *Output current control*

For the implementation of FRT control systems, usually, the measured currents and voltages have to be separated into positive and negative sequence components. To achieve sequence separation, Delayed-signal-cancellation (DSC) is probably the best-suited method [9], but has an intrinsic delay of 5ms (for ω_g=50Hz) before achieving the separation of the sequence components. To reduce the inherent delay present in traditional DSC, the fast convergence DSC proposed in [10] is utilised in this work to calculate the sequence components.

As is reported in [11], the currents, the powers and the voltages are related by:

$$\begin{bmatrix} P_{\mathrm{g}} \\ Q_{\mathrm{g}} \\ P_{fs2} \\ P_{fc2} \end{bmatrix} = \begin{bmatrix} v_{g\alpha}^p & v_{g\beta}^p & v_{g\alpha}^n & v_{g\beta}^n \\ v_{g\beta}^p & -v_{g\alpha}^p & v_{g\beta}^n & -v_{g\alpha}^n \\ v_{g\beta}^n & -v_{g\alpha}^n & -v_{g\beta}^p & v_{g\alpha}^p \\ v_{g\alpha}^n & v_{g\beta}^n & v_{g\alpha}^p & v_{g\beta}^p \end{bmatrix} \begin{bmatrix} i_{g\alpha}^p \\ i_{g\beta}^p \\ i_{g\alpha}^n \\ i_{g\beta}^n \end{bmatrix} \quad (21)$$

Where the superscripts p, and n are utilised to symbolise the positive and negative sequence components, respectively. The terms "P_{fs2}" and "P_{fc2}" represents double frequency oscillations in active power that can be mitigated considering the next current reference calculation:

$$\begin{bmatrix} i_{g\alpha}^{p*} \\ i_{g\beta}^{p*} \\ i_{g\alpha}^{n*} \\ i_{g\beta}^{n*} \end{bmatrix} = \begin{bmatrix} v_{g\alpha}^p & v_{g\beta}^p & v_{g\alpha}^n & v_{g\beta}^n \\ v_{g\beta}^p & -v_{g\alpha}^p & v_{g\beta}^n & -v_{g\alpha}^n \\ v_{g\beta}^n & -v_{g\alpha}^n & -v_{g\beta}^p & v_{g\alpha}^p \\ v_{g\alpha}^n & v_{g\beta}^n & v_{g\alpha}^p & v_{g\beta}^p \end{bmatrix}^{-1} \begin{bmatrix} P_g^* \\ Q_g^* \\ 0 \\ 0 \end{bmatrix} \quad (22)$$

Because of Resonant Controllers (RC) can be used to regulate positive and negative sequence current at the same time, only two RC are needed instead of four for d-q axis based control systems [11], [12]. Therefore, this type of regulators is applied to output current control. At this point and considering (3), voltage references to achieve decoupled output current control using RC can be calculated as:

$$\begin{bmatrix} v_{0\alpha}^* \\ v_{0\beta}^* \end{bmatrix} = \begin{bmatrix} v_{g\alpha} \\ v_{g\beta} \end{bmatrix} - L_{22}\frac{d}{dt}\begin{bmatrix} i_{g\alpha} \\ i_{g\beta} \end{bmatrix} - C_{RC_{out}}(s)\left(\begin{bmatrix} (i_{g\alpha}^{p*} + i_{g\alpha}^{n*}) \\ (i_{g\beta}^{p*} + i_{g\beta}^{n*}) \end{bmatrix} - \begin{bmatrix} i_{g\alpha} \\ i_{g\beta} \end{bmatrix}\right) \quad (23)$$

Where $G_{RC_{out}}(s)$ represents the Output Current Resonant Controller transfer function.

D. *Cell balancing Method and Modulation*

The voltage references obtained in control loops presented abode ($v_{\alpha\alpha}^*, v_{\beta\alpha}^*, v_{\alpha\beta}^*, v_{\beta\beta}^*, v_{\alpha 0}^*, v_{\beta 0}^*, v_{0\alpha}^*, v_{0\beta}^*$) are transformed to the natural reference frame using the two stage inverse $\alpha\beta 0$-Transformation.Then, an AC voltage reference is obtained for each branch: $v_{ar}^*, v_{br}^*, v_{cr}^*, v_{as}^*, v_{bs}^*, v_{cs}^*, v_{at}^*, v_{bt}^*, v_{ct}^*$.

An additional control loop is utilised to ensure equal dc capacitor voltages within a branch [13]. The voltage reference "v_{xy}^*" is distributed among the number of cells in the $x-y$ branch. The capacitor voltage for the cell number *"i"*, with $i \in (1, n)$, is compared with the desired value "$\bar{v}_c^o$". Then, the error is multiplied for the sing of the branch current, resulting in the addition/subtraction of a ΔV to the cell voltage reference.

Finally, the phase-shifted PWM is used to synthesise the multilevel waveforms. It has been validated that the phase-shifted PWM is easy to enlarge the count of bridge cells per cluster, the power losses are equally distributed in the cell of the same branch. Moreover, using phase-shifted unipolar modulation, the output switching frequency is *2*3n* times the triangular carrier frequency.

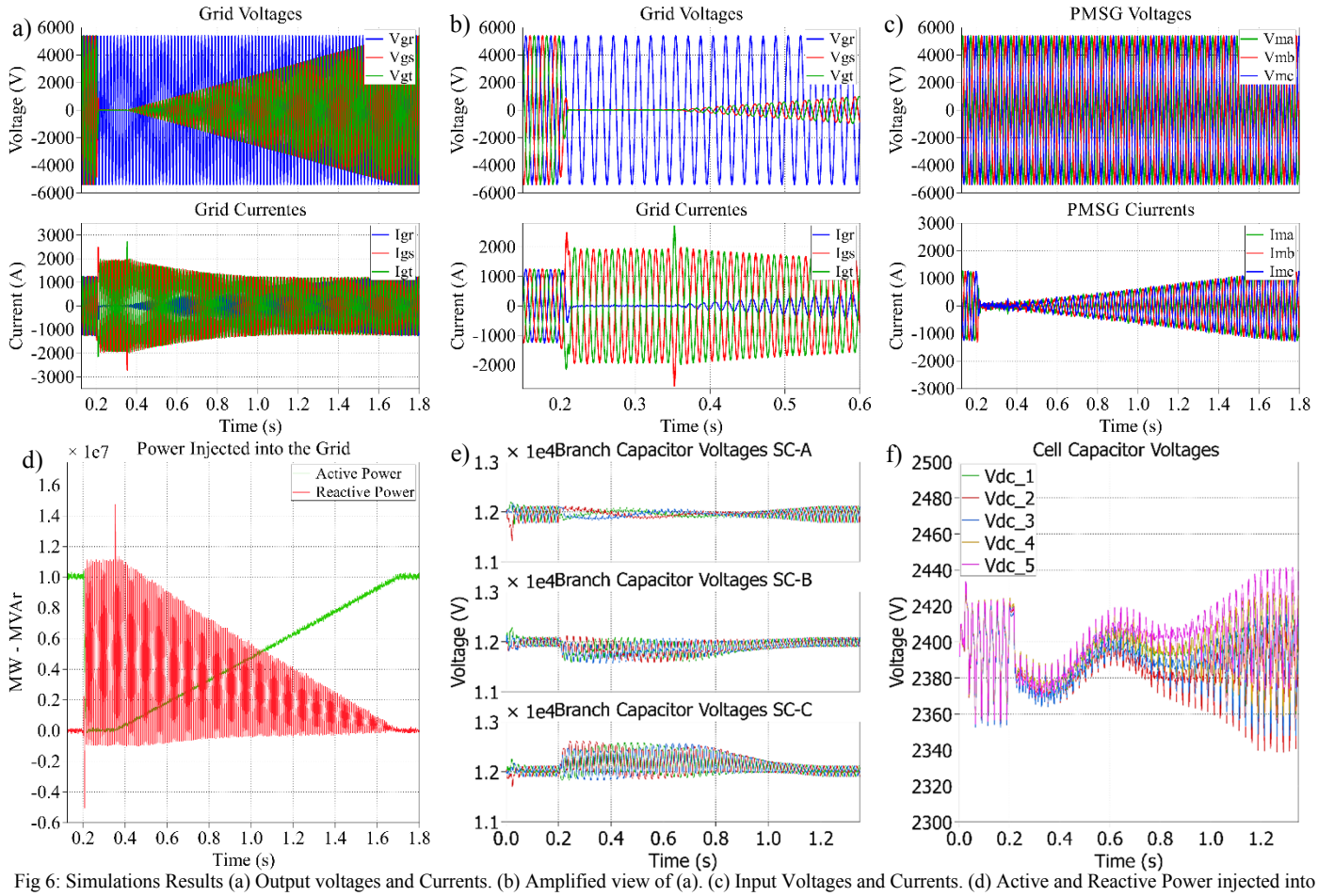

Fig 6: Simulations Results (a) Output voltages and Currents. (b) Amplified view of (a). (c) Input Voltages and Currents. (d) Active and Reactive Power injected into the grid. (e) Average Branch Capacitor Voltages for SubConver A, B and C, respectively. (f) Capacitor Voltages, branch "a-s".

V. Simulation and Experimental Results

The effectiveness of the proposed control strategy has been tested through simulation and experimental work. The simulations have been developed using PLECS software, considering a five cell per branch M3C connected to the grid. The general parameters of the simulated model are depicted in Table I. This system has been tested under variable speed operation and grid-voltage dips to validate the novel application of M3C driving high-power grid-connected WECS.

Table I: Simulation Parameters

Nominal Power	10 MW
Cells per branch	5
Input Voltage/Freq,	5.4kV/10-40Hz
Branch Inductor	2.5 mH
Cap. in each cell	2.8 mF
Capacitor Voltage	2.4 kV
Output Voltage/Freq.	5.4kV/60 Hz
Switching frequency	0.8kHz

Table II: Experimental Setup

Nominal Power	5 kW
Cells per branch	3
Input Voltage/Freq,	200V/10-40Hz
Branch Inductor	2.5 mH
Cap. in each cell	4.7 mF
Capacitor Voltage	155V
Output Voltage/Freq.	185V/50 Hz
Switching frequency	2.5kHz

The performance of the proposed control strategy is tested for a Dip Type C (two phases decrease their nominal voltage to 0V) based on the regulations present in the German grid code [5], as is shown in Fig. 6(a) and Fig 6(b). When the fault appears, the input current control stops the active power generation by reducing the current to zero (Fig. 6(c)). The output currents are controlled using the calculation presented in (22), which generates unbalanced references to mitigating the effects of the grid voltage dip and provide full reactive power injection, as is shown in Fig.6(d). There are not double-frequency oscillations in active power, but reactive power presents double frequency oscillations that cannot be controlled because there are not enough degrees of freedom [12]. As is presented in Fig. 6(e) and Fig. 6(f), proper energy balancing is achieved through the grid voltage dip.

Experimental results have been obtained with downscaled laboratory prototype, composed of nine branches, each of them considering the series connection of 3 H-Bridge modules and 1 cluster inductor. The system is controlled using one Digital Signal Processor (DSP) Texas Instrument TMS320C6713 and three Actel ProAsic3 field programmable gate array (FPGA) boards equipped with 50 14-bit analogue-digital channels. The 108 switching signals are obtained in the FPGA boards using unipolar phase-shifted PWM and are transmitted using fibre optic communications. More details about the experimental prototype are depicted in Table II, and a picture of the system is shown in Fig. 7(a).

The synchronised operation of the experimental prototype is presented in Fig. 7(b). The M3C is controlled to operate with unitary power factor, injecting 3.5kW into the grid. Waveforms of the phase-to-phase voltage between phases r-t are shown in the upper and middle waveforms of Fig. 7(b). Both voltages are controlled to 185V (peak phase-to-neutral value), and the grid current is controlled to 12A (peak value).

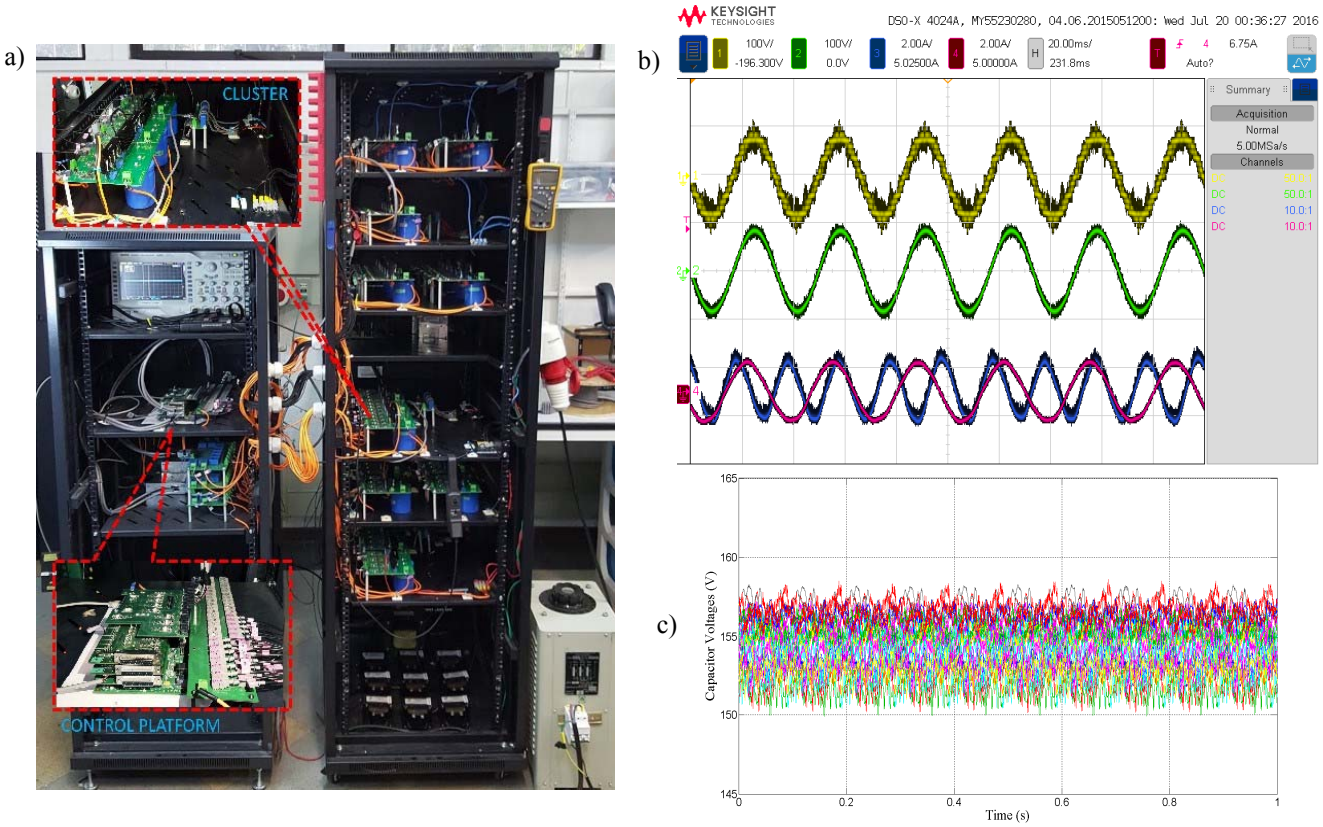

Fig. 7: (a) Experimental Prototype. (b) Experimental Results. Upper: Line-to-Line Output Voltage phase r-t, 400V/div. Middle: Line-to-Line Grid Voltage phase r-t, 400V/div. Lower: Grid current (purple), Input Current (Blue), 10A/div

Additionally, the input and output currents are presented to illustrate the frequencies operation (30Hz at the output and 50Hz at the input). The 27 capacitor voltages have been measured using the capabilities of the control platform and are presented in Fig. 7(c). The average voltage is regulated to 155V, and is observed that the ripple is lower than +-4V.

VI. CONCLUSIONS

A fully decoupled control strategy for the application of the Modular Multilevel Matrix Converter in high-power WECS has been proposed in this paper. Beyond the current state of the art, WECS based on the Modular Multilevel Matrix Converter is a novel topology that could be applied successfully in high power wind turbines.

The proposed decoupled control strategy enables independent current and energy balancing regulation, by using the electrical circuit transformation based on the two-stage $\alpha\beta 0$ transformation.

Experimental results obtained with a 27H-Bridges Prototype and Simulation tests have been carried out to validate the effectiveness of the proposed control strategy for wind energy applications. In fact, the proposed control approach could be suitable for a wider range of electrical machine applications.

VII. REFERENCES

[1] Global Wind Energy Council, "Global Wind Statistics 2015," 2015.

[2] N. Fichaux, J. Beurskens, and P. Jensen, "Upwind: Design limits and solutions for very large wind turbines," 2011.

[3] A. Mora, M. Espinoza, M. Diaz, and R. Cardenas, "Model Predictive Control of Modular Multilevel Matrix Converter," in *2015 IEEE 24th International Symposium on Industrial Electronics (ISIE)*, 2015, pp. 1074–1079.

[4] J. Korn, M. Winkelnkemper, P. Steimer, and J. W. Kolar, "Direct modular multi-level converter for gearless low-speed drives," in *Proceedings of the 2011 14th European Conference on Power Electronics and Applications*, 2011, no. direct MMC, pp. 1–7.

[5] F. Iov, A. D. Hansen, P. Sørensen, and N. A. Cutululis, "Mapping of grid faults and grid codes," *Wind Energy*, vol. 1617, no. July, pp. 1–41, 2007.

[6] A. Korn, M. Winkelnkemper, P. Steimer, and J. W. Kolar, "Direct modular multi-level converter for gearless low-speed drives." pp. 1–7, 2011.

[7] F. Kammerer, J. Kolb, and M. Braun, "Fully decoupled current control and energy balancing of the Modular Multilevel Matrix Converter," in *15th International Power Electronics and Motion Control Conference and Exposition, EPE-PEMC 2012 ECCE Europe*, 2012, pp. LS2a.3–1–LS2a.3–8.

[8] W. Kawamura, M. Hagiwara, and H. Akagi, "Control and Experiment of a Modular Multilevel Cascade Converter Based on Triple-Star Bridge Cells," *IEEE Trans. Ind. Appl.*, vol. 50, no. 5, pp. 3536–3548, Sep. 2014.

[9] S. Alepuz, S. Busquets-Monge, J. Bordonau, J. A. Martinez-Velasco, C. A. Silva, J. Pontt, and J. Rodriguez, "Control Strategies Based on Symmetrical Components for Grid-Connected Converters Under Voltage Dips," *IEEE Trans. Ind. Electron.*, vol. 56, no. 6, pp. 2162–2173, Jun. 2009.

[10] R. Cardenas, M. Diaz, F. Rojas, and J. Clare, "Fast Convergence Delayed Signal Cancellation Method for Sequence Component Separation," *IEEE Trans. Power Deliv.*, vol. 30, no. 4, pp. 2055–2057, Aug. 2015.

[11] M. Diaz, R. Cardenas, P. Wheeler, J. Clare, and F. Rojas, "Resonant Control System for Low-Voltage Ride-Through in Wind Energy Conversion Systems," *IET Power Electron.*, pp. 1–16, Feb. 2016.

[12] M. Diaz and R. Cardenas, "Analysis of synchronous and stationary reference frame control strategies to fulfill LVRT requirements in Wind Energy Conversion Systems," in *2014 Ninth International Conference on Ecological Vehicles and Renewable Energies (EVER)*, 2014, pp. 1–8.

[13] H. Akagi, S. Inoue, and T. Yoshii, "Control and Performance of a Transformerless Cascade PWM STATCOM With Star Configuration," *IEEE Trans. Ind. Appl.*, vol. 43, no. 4, pp. 1041–1049, 2007.